Electronic Supplementary Information for

2D boron nitride nanoflakes as a multifunctional additive in gel polymer electrolyte for safe, long cycle life and high rate lithium metal batteries

Jimin Shim,[a] Hee Joong Kim,[a] Byoung Gak Kim,[bc] Yong Seok Kim,[bc] Dong-Gyun Kim,[*bc] and Jong-Chan Lee[*a]

[a] School of Chemical and Biological Engineering and Institute of Chemical Processes, Seoul National University, 599 Gwanak-ro, Gwanak-gu, Seoul 08826, Republic of Korea.
[b] Advanced Materials Division, Korea Research Institute of Chemical Technology, 141 Gajeong-ro, Yuseong-gu, Daejeon 34114, Republic of Korea.
[c] Chemical Convergence Materials and Processes, University of Science and Technology, 217 Gajeong-ro, Yuseong-gu, Daejeon 34114, Republic of Korea.

**Corresponding author: D.-G. Kim (E–mail: dgkim@krict.re.kr)*
J.-C. Lee (E–mail: jongchan@snu.ac.kr)

Table of Contents

Experimental Section

Materials

Krytox® acid ($F(CF(CF_3)CF_2O)_nCF(CF_3)COOH$, n=14.1) was received from Dupont. Hexagonal boron nitride (BN, MK-hBN-N70, Lower Friction), poly(vinylidene fluoride-*co*-hexafluoropropylene) (PVH) (product / CAS number: 427179 / 9011-17-0, dielectric constant = 9.0-10.0 at 100 Hz (ASTM D 150), average M_n = 110,000 g mol^{-1}, M_w = 455,000 g mol^{-1}), 1-pyrenemethanol, and thionyl chloride were purchased from Aldrich and used as received. Methoxynonafluorobutane was purchased from TCI and stored over 3 Å molecular sieves prior to use. 1.0 M lithium bis(trifluoromethane sulfonyl)imide (LiTFSI) in a mixture of ethylene carbonate (EC) and diethylene carbonate (DEC) (1:1 vol%) was purchased from PANAXETEC. Co., Ltd. Microporous polyolefin membrane (Celgard, 25 μm thickness, PE/PP/PE trilayer, Celgard®2325) was obtained from Celgard, LLC and used for comparison purposes. All other reagents and solvents were obtained from reliable commercial sources and used as received.

Synthesis of pyrene with a perfluoropolyether chain (PFPE-Pyrene)

Krytox® acid (5.0 g, 2.0 mmol) was dissolved in 20 mL of methoxynonafluorobutane and the resultant solution was added to a 100 mL of two-neck round bottomed flask equipped with a condenser and a magnetic stirring bar. The solution was heated at 60 °C for 1 h in an oil bath under nitrogen atmosphere. Thionyl chloride (0.48 g, 4.0 mmol) and pyridine (0.079 g, 1.0 mmol) were added to the solution and stirred for 16 h. To obtain the product, the resultant salt was removed by vacuum filtration and the excessive thionyl chloride was evaporated at 60 °C under vacuum using rotary evaporator. After further dried under vacuum at room temperature for 24 h, the Krytox® acid with acyl chloride functional group (3.0 g, 1.2 mmol) in 7 mL of methoxynonafluorobutane was added to a 50 mL of two-neck round bottomed flask equipped with a condenser and a magnetic stirring bar. 1-Pyrenemethanol (0.33 g, 1.43 mmol) in 7 mL of chloroform was then added to the flask by a syringe, followed by the addition pyridine (0.094 g, 1.2 mmol). The reaction mixture was stirred at 60 °C for 20

h under nitrogen atmosphere. The residual solvents were removed by evaporation, and the crude product was precipitated in methanol several times. After being dried under vacuum at room temperature for 24 h, bright yellowish oil was obtained with 58 % yield.

Preparation of boron nitride nanoflakes noncovalentely functionalized with PFPE-Pyrene (FBN)

BN (0.1 g) and PFPE-Pyrene (0.1 g) were sonicated in 100 mL of methoxynonafluorobutane for 10 h. The dispersed mixture was centrifuged at 3000 rpm for 15 min three times and the supernant was collected. After the residual solvent was removed by evaporation, slightly yellow powder was obtained with 5 % yield.

Preparation of composite gel polymer electrolytes (GPEs)

FBN was added to 10 wt% of PVH in acetone and the mixture was sonicated for 3 h. The amount of FBN was controlled as 0.1, 0.2, 0.5, and 1.0 wt% of the PVH. The dispersion was cast onto a glass plate using a doctor blade and dried at ambient condition. The obtained membrane was peeled from the glass plate and further dried at 60 ^{o}C under high vacuum for several days. The membrane was then immersed in 1.0 M LiTFSI in EC:DEC (1:1 vol%) for 24 h inside a glove box to prepare gel polymer electrolyte.

Instrumentation and characterization techniques

^{19}F NMR spectra were recorded on a JeolJNM-LA400 spectrometer (400 MHz) with LFG. $CDCl_3$ (containing TMS as a reference, Cambridge Isotope Laboratories), mixed with methoxynonafluorobutane, was used as a solvent. The Fourier transform infrared (FT-IR) spectra were recorded in the absorption mode on Nicolet 6700 spectrophotometer with a resolution of 4 cm^{-1} in the vibrational frequency range from 400 to 4000 cm^{-1}. Field-emission scanning electron microscopy (FE-SEM) was performed on a JEOL JSM-6700F with an accelerating voltage of 10 kV. Transmission

electron microscopy (TEM) was performed on a LIBRA 120 with an accelerating voltage of 120 kV. TEM specimens were prepared by drop casting of 0.1 wt % dispersion in acetone on carbon-coated grid. The morphology of FBN was observed using atomic force microscopy (AFM, Asylum Research MFP-3D) in tapping-mode under ambient condition. The X-ray diffraction (XRD) spectra were obtained using Rigaku SmartLab (Cu Kα) spectrometers. Raman spectra were collected on a T64000 Triple Raman spectrometer (HORIBA) equipped with a 532 nm Ar laser source. The mechanical properties were measured using a universal testing machine (UTM, LS1SC, LLOYD Instruments). UTM specimens were prepared following the ASTM standard D638 (Type V specimens dog-bone shaped samples). The tensile properties of the membrane samples were measured with a gauge length and cross head speed of 15 mm and 5 mm min^{-1}, respectively. At least five specimens for each sample were tested and their average values were used. The amount of liquid electrolyte uptake was determined by measuring their changes in weight before and after immersion in the liquid electrolyte for 24 h. The electrolyte uptake value is calculated as follows:

$$\text{Electrolyte uptake (\%)} = [(W_{wet}-W_{dry})/W_{dry}] \times 100 \quad (1)$$

where W_{dry} and W_{wet} is the weight of membrane before and after immersion in liquid electrolyte, respectively.

Electrochemical characterization

The ionic conductivities of GPEs at 25 °C were determined using complex impedance spectroscopy with a Zahner Electrik IM6 apparatus in the frequency range of 0.1 Hz to 1.0 MHz with 10 mV of AC amplitude. The samples for the measurements were prepared by sandwiching the GPEs between two stainless-steel electrodes in a 2032 coin cell. The ionic conductivity (σ) was calculated from the following equation (2):

$$\sigma = (1/R) \times (d/A) \quad (2)$$

where R is the electrolyte resistance obtained from the impedance spectrum, d is the thickness of electrolyte, and A is the area of the electrode. Li^+ transference number (t_{Li^+}) was determined by DC polarization/AC impedance combination method at 25 °C. The GPEs were sandwiched between two non-blocking lithium metal disks to form a symmetrical Li/GPE/Li in 2032 coin cell. The cell was polarized by a constant DC voltage of 10 mV and following current values were monitored until steady-state current was observed. The initial and steady-state resistances of the cell were also measured. From this method, t_{Li^+} was determined by the following equation (3):

$$t_{Li^+} = [I_s \times (V - I_i \times R_i)] / [I_i \times (V - I_s \times R_s)] \quad (3)$$

where V is constant DC voltage applied to the cell and R_i and R_s are initial and steady-state resistances, respectively. I_i and I_s are initial and steady-state currents, respectively. Galvanostatic charge/discharge test was carried out to evaluate dendrite-suppressing behaviour at 25 °C. Time evolution of voltage profiles was measrured on a symmetric Li/Li cell during repetitive charge/discharge cycles, where the cell was cycled under constant current density of 1.0 mA cm^{-2} and the polarity was reversed for every 3 h. Charge/discharge cycling test of lithium metal battery (LMB) was performed with WBCS3000 battery cycler (WonATech). $LiFePO_4$ (80 wt%, LG Chem, Ltd) was used as cathode active materials and dispersed in *N*-methyl-2-pyrrolidone (NMP) with carbon black (10 wt%) and PVdF (10 wt%). The resultant slurry was deposited and cast onto an aluminium current collector using a doctor blade. The residual NMP was completely removed under vacuum condition at 120 °C for 24 h. The obtained cathode sheet, lithium metal, and GPE were punched into disk shapes and assembled together in a 2032 coin cell to form Li/GPE/$LiFePO_4$ cell. All components were assembled in argon filled glove box (H_2O < 0.5 ppm, O_2 < 0.5 ppm). Charge/discharge cycling test of the LMB was performed at cutoff voltages of 2.5–4.2 V *vs.* Li/Li^+ at 25 °C with C-rates of 1.0 C and 10 C, where the 1.0 C rate corresponds to a current density of 170 mA g^{-1}. Rate capability of Li/GPE/$LiFePO_4$ cell was also tested at the same cutoff voltages at 25 °C by varying the current densities.

Synthesis of Pyrene with a Perfluoropolyether Chain (PFPE-Pyrene)

PFPE-Pyrene was synthesized by esterification between PFPE-COOH and 1-pyrenemethanol as shown in Fig. S1. Carboxylic acid group of PFPE-COOH was activated by thionyl chloride and subsequently reacted with 1-pyrenemethanol. The structure of products in each step was characterized by FT-IR spectroscopy (Fig. S2). The wavenumbers of carbonyl (C=O) peaks of PFPE-COOH, PFPE-COCl, and PFPE-Pyrene are slightly changed as the reaction proceeds, indicating the successful conversion. Furthermore, PFPE-Pyrene has C=C strecthing peaks from aromatic pyrene moieties. Fig. S3 shows ^{19}F NMR spectra of PFPE-COOH, PFPE-COCl, and PFPE-Pyrene. PFPE-COOH has a peak at -132 ppm that is associated with a fluorine atom adjacent to the carbonyl group. This fluorine peak is shifted as the reaction proceeds (-126 ppm and -133 ppm for PFPE-COCl and PFPE-Pyrene, respectively).

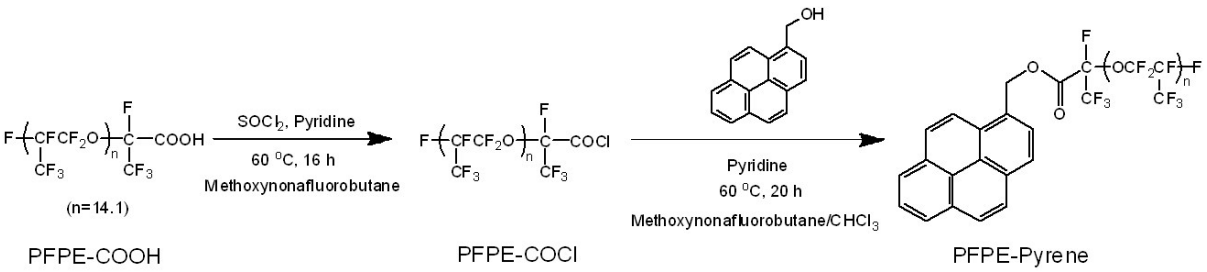

Fig. S1 Synthesis of PFPE-Pyrene.

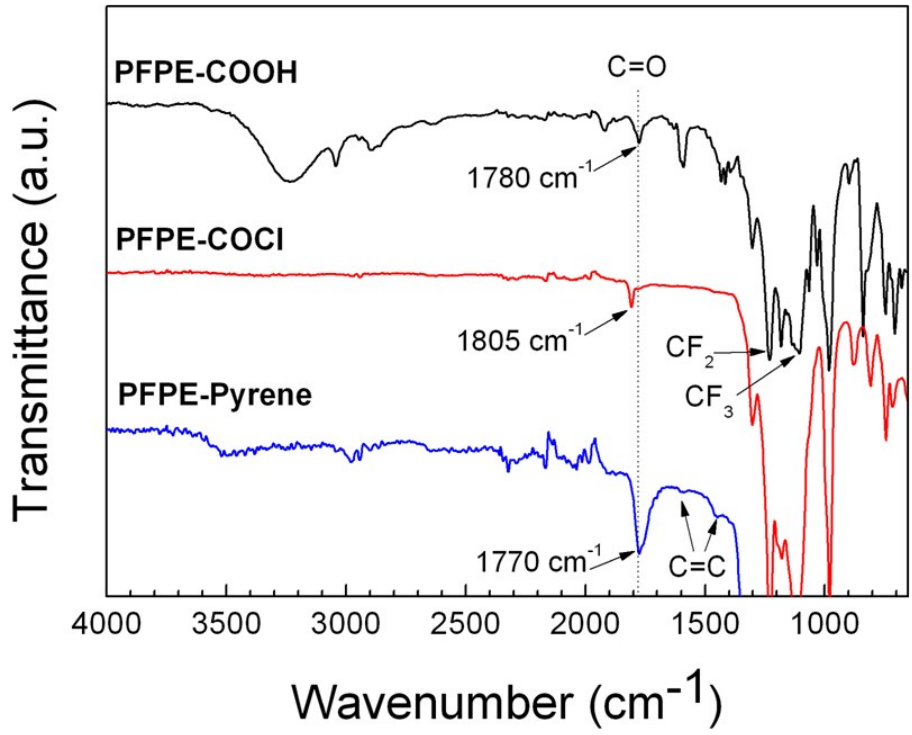

Fig. S2 FT-IR spectra of PFPE-COOH, PFPE-COCl, and PFPE-Pyrene.

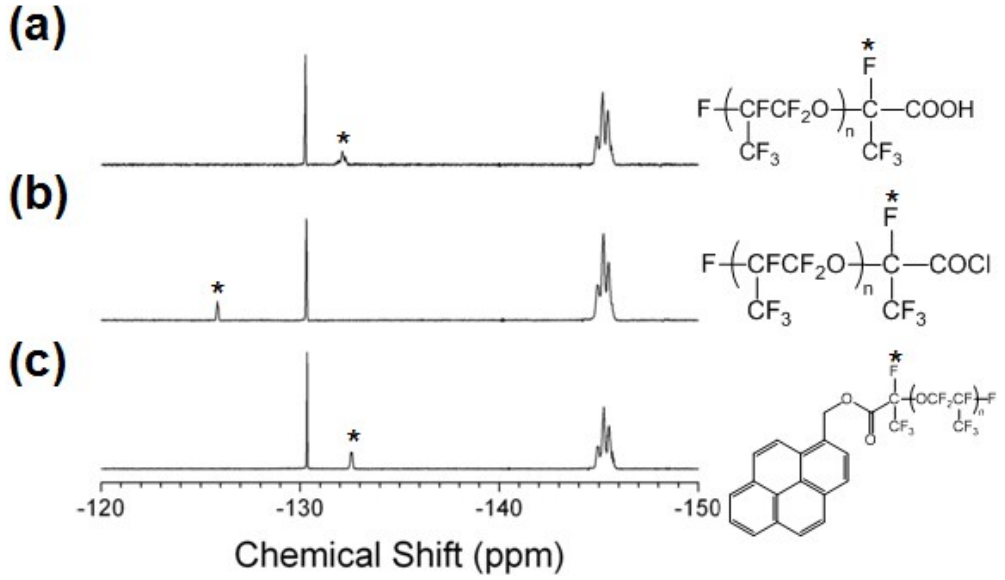

Fig. S3 ^{19}F-NMR spectra of (a) PFPE-COOH, (b) PFPE-COCl, and (c) PFPE-Pyrene.

Preparation and Structural Characterization of FBN

FBN was prepared via sonication-assisted exfoliation and noncovalent functionalization of BN powder by PFPE-Pyrene as shown in Fig. S4. BN can be readily functionalized by the noncovalent functionalization without losing any intrinsic properties of BN, while covalent functionalization based on chemical reactions deteriorates the intrinsic properties of the BN. Stacked BN layers are exfoliated during the sonication process and the electron-deficient BN surface is noncovalently functionalized by electron-rich PFPE-Pyrene at the same time. The PFPE chains are introduced to induce autonomous pore formation via phase separation between the FBN-incorporated PVH matrix and acetone, even without addition of any porogen or non-solvent, thereby improving electrolyte uptake ability. Nano-sized BN was used for the preparation of FBN as shown in Fig. S5 to utilize its large surface area and good dispersion behaviour in the polymer matrix.

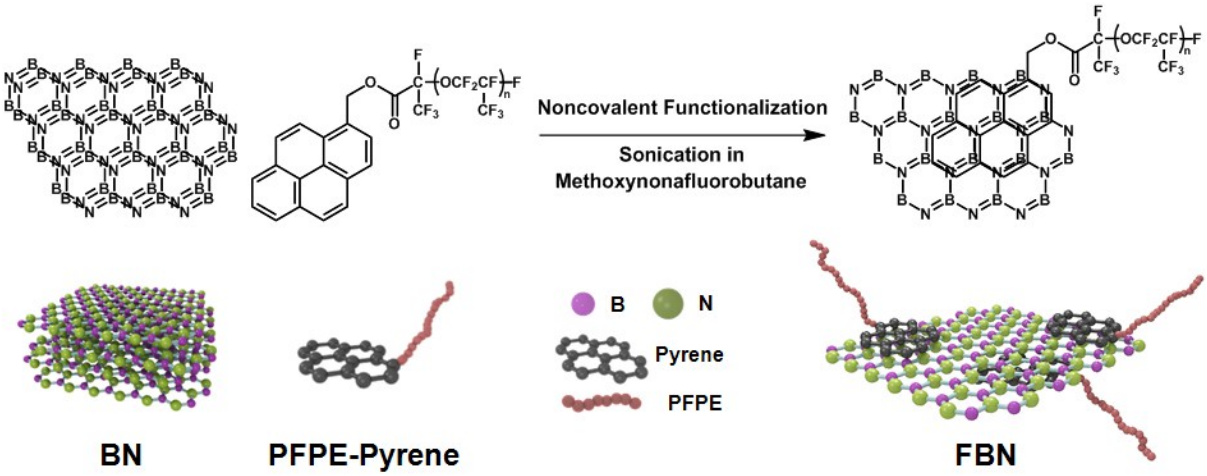

Fig. S4 Preparation of FBN *via* sonication-assisted noncovalent functionalization.

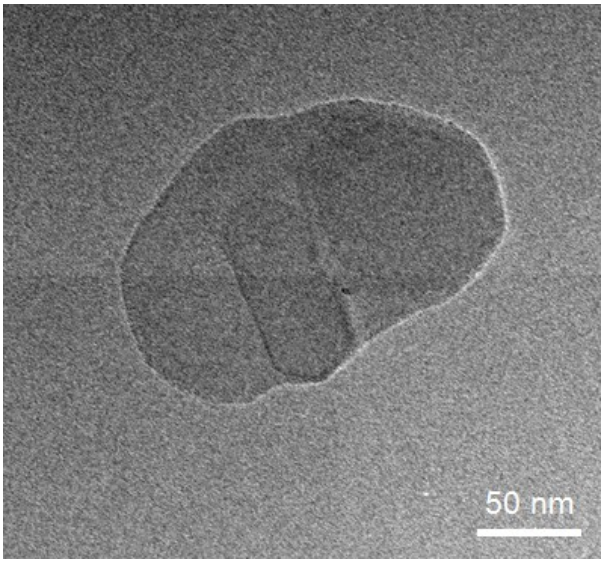

Fig. S5 HR-TEM image of BN.

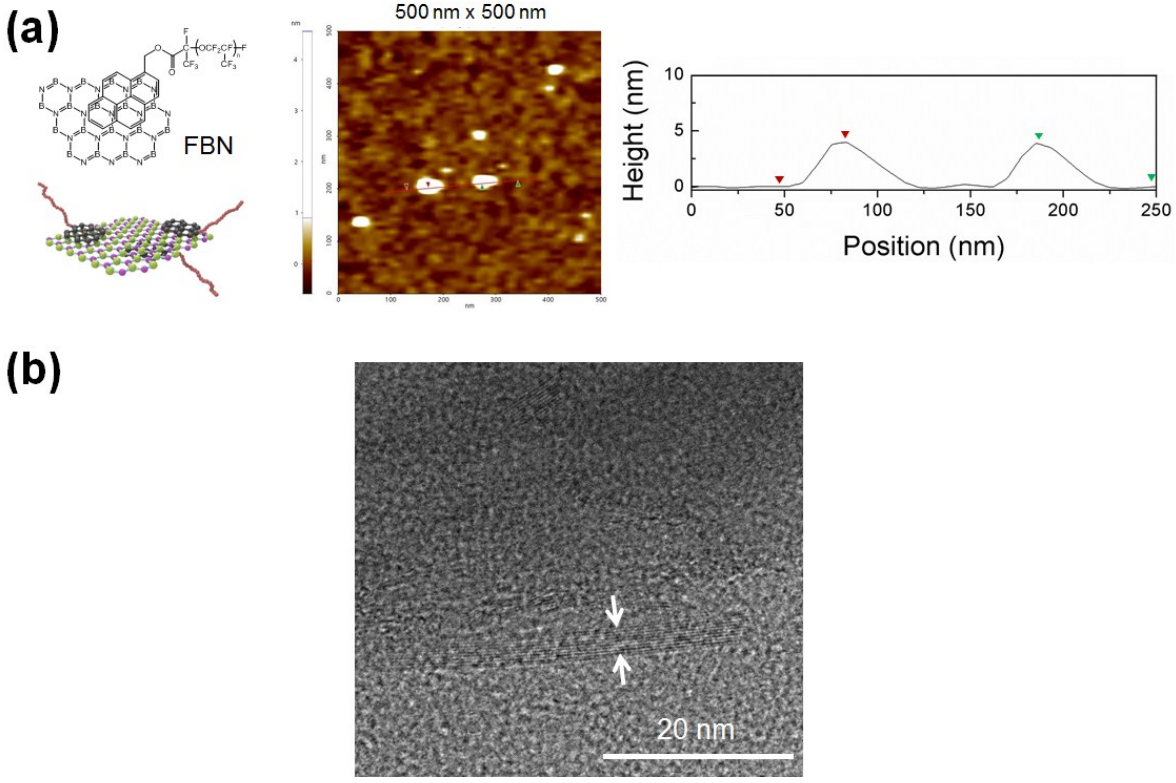

Fig. S6 (a) AFM topography image and line-scan profile and (b) HR-TEM image of FBN.

The exfoliation state of FBN was confirmed by AFM and HR-TEM analyses. As shown in Fig. S6a, the thickness of FBN is about 3–4 nm that is much decreased from that of pristine BN (40-60 nm), indicating that pristine BN layers are exfoliated during the sonication-assisted noncovalent functionalization. As shown in HR-TEM image in

Fig. S6b, several fringes were observed at folded edges of FBN layers and their thicknesses are in the range of 3–4 nm on average, indicating that FBN has exfoliated 9–12 BN layers, as also estimated from the AFM result.

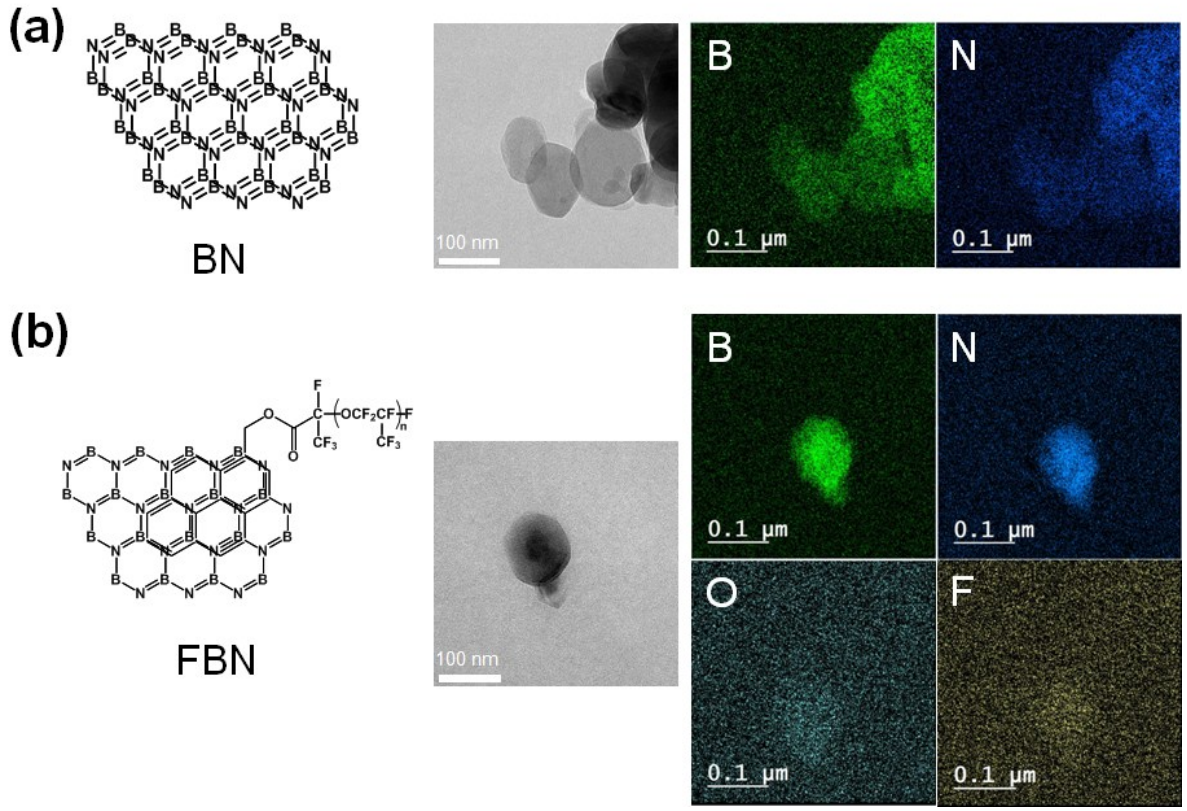

Fig. S7 TEM images and electron energy loss spectra of (a) BN and (b) FBN.

Fig. S7 shows TEM images and electron energy loss spectra of BN and FBN. Both BN and FBN have B and N signals from the BN. In addition, FBN has O and F signals from PFPE chains, indicating the successful noncovalent functionalization. Since the amount of PFPE chains in the FBN is relatively small compared to that of BN in the FBN, thick, aggregated FBN layers were intentionally chosen for the analysis (Fig. S7b).

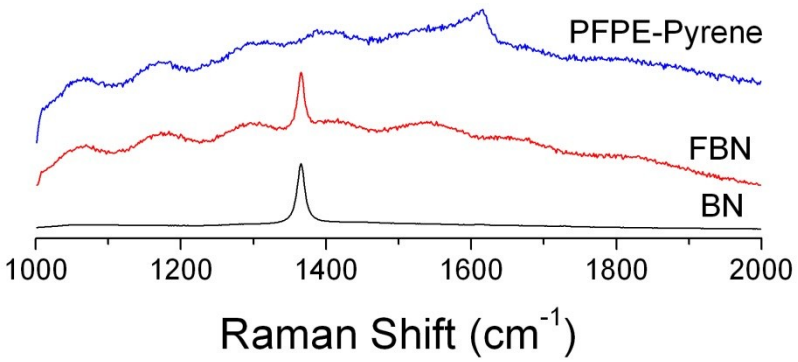

Fig. S8 Raman spectra of BN, FBN, and PFPE-Pyrene.

Fig. S8 shows Raman spectra of BN, FBN, and PFPE-Pyrene. The band at 1367 cm^{-1} indicates E_{2g} phonon mode of B-N, which appears in both BN and FBN spectra. In the case of FBN, Raman bands from PFPE chain are also observed, indicating that PFPE chains were successfully attached to the BN surface. The bands at 1067/1072 cm^{-1} and 1299 cm^{-1} correspond to symmetric CF_2 and CF_3 strecthing modes of PFPE chain, respectively. The two bands at 1400 and 1610 cm^{-1} are attributed to the aromatic C=C stretching mode of pyrene moieties.

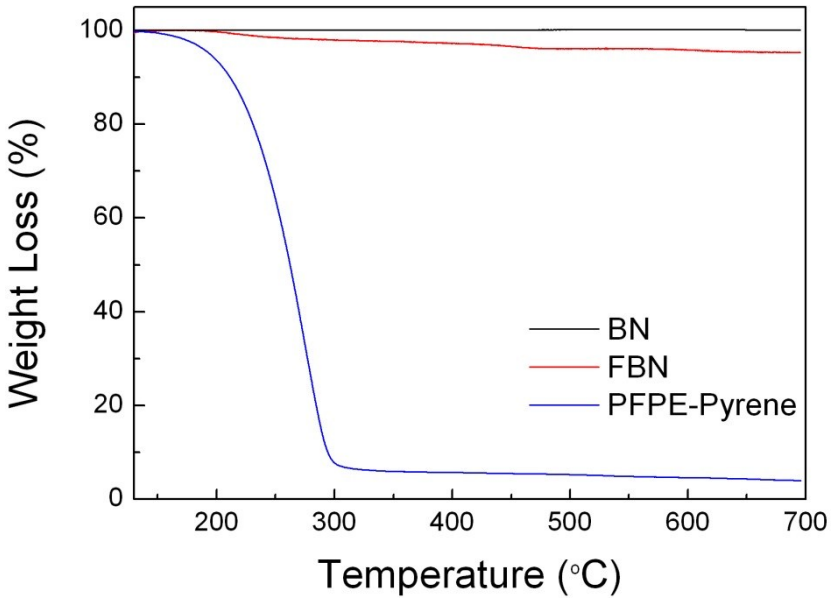

Fig. S9 TGA profiles of BN, FBN, and PFPE-Pyrene.

The TGA profiles in Fig. S9 provide additional information on FBN composition. BN shows good thermal stability without any weight loss up to 700 ^{o}C, while the weight of FBN continuously decreases due to the decomposition of PFPE-Pyrene which is noncovalently attached to the BN. The final weigtht loss of FBN at 700 ^{o}C is found to be about 4.7 wt%. Since the non-zero char yield of PFPE-Pyrene at 700 ^{o}C is ascribed to the presence of aromartic pyrene moieties, it can be estimated that the amount of noncovalently attached PFPE-Pyrene is slightly larger than 4.7 wt%.

Preparation of Gel Polymer Electrolytes

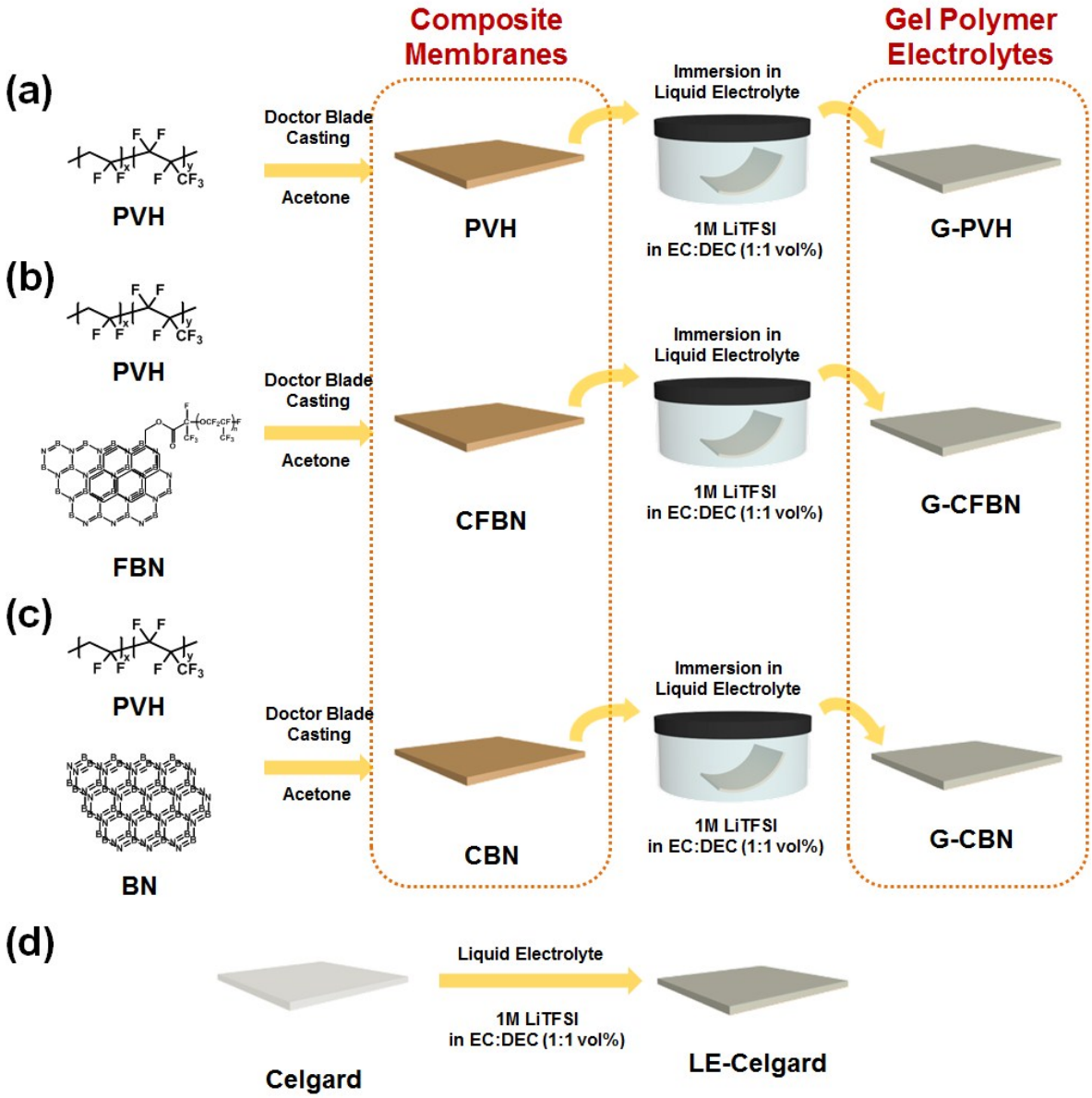

Fig. S10 Schematic illustration of preparation of (a) G-PVH, (b) G-CFBN, (c) G-CBN, and (d) LE-Celgard.

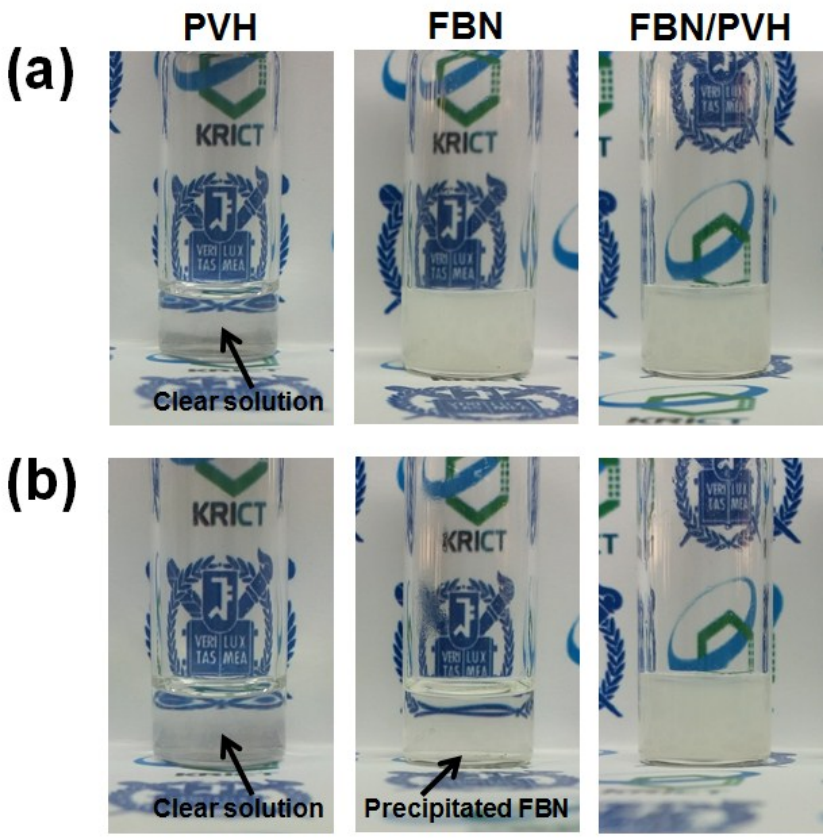

Fig. S11 Dispersion state of PVH, FBN, and FBN/PVH (left to right) in acetone (a) right after sonication and (b) after 1 h.

The concentration of each sample is identical with that of the casting solution in membrane preparation. 10 wt% of PVH dissolved in acetone was used, and the amount of FBN was controlled as 0.5 wt% of the PVH. For the sample with FBN only, the same amount of FBN in the FBN/PVH sample was placed in acetone.

Morphology of Composite Membranes

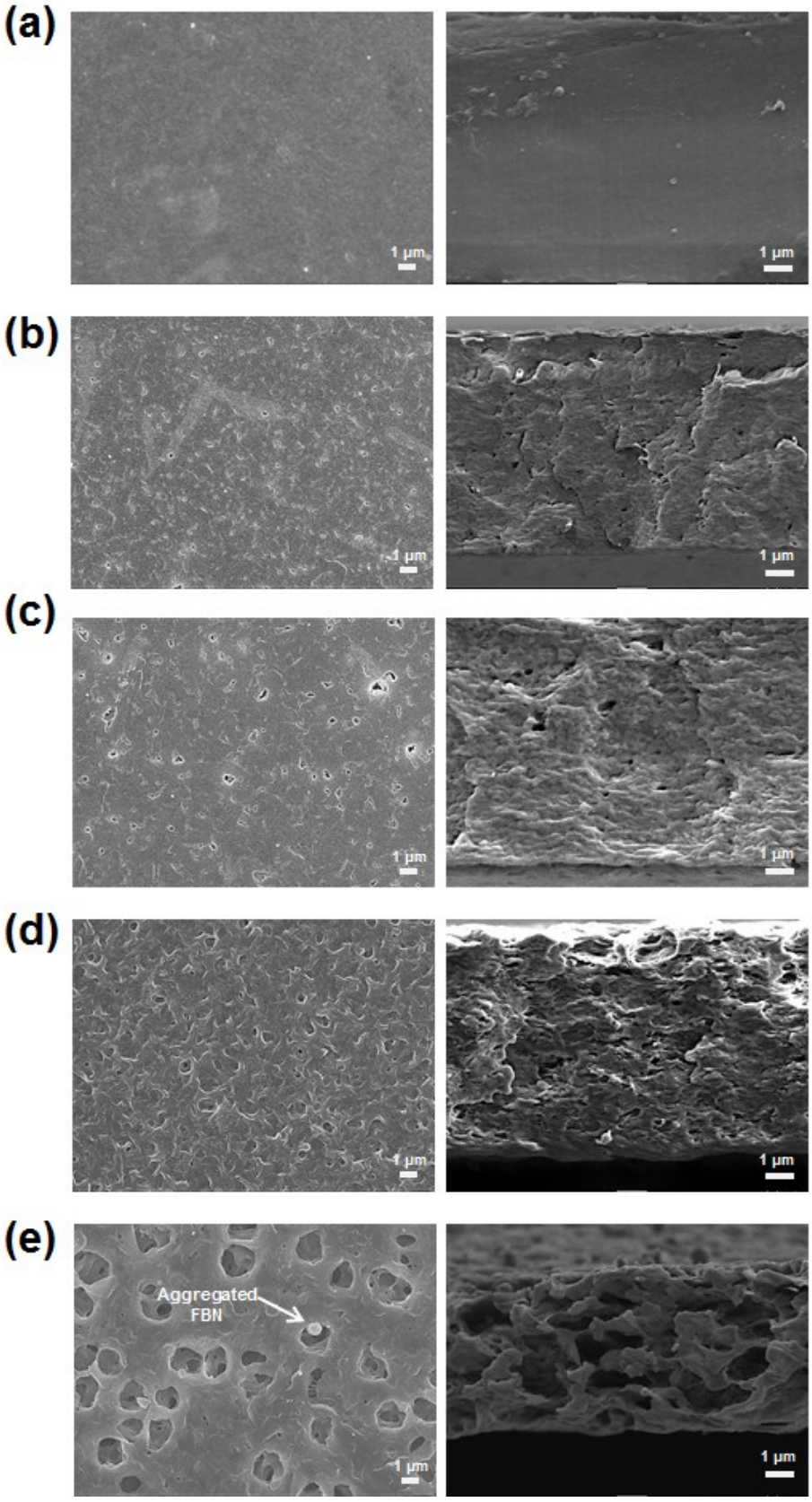

Fig. S12 Surface (left) and cross-sectional (right) SEM images of (a) PVH, and CFBNs with (b) 0.1 wt%, (c) 0.2 wt%, (d) 0.5 wt%, and (e) 1.0 wt% of FBN.

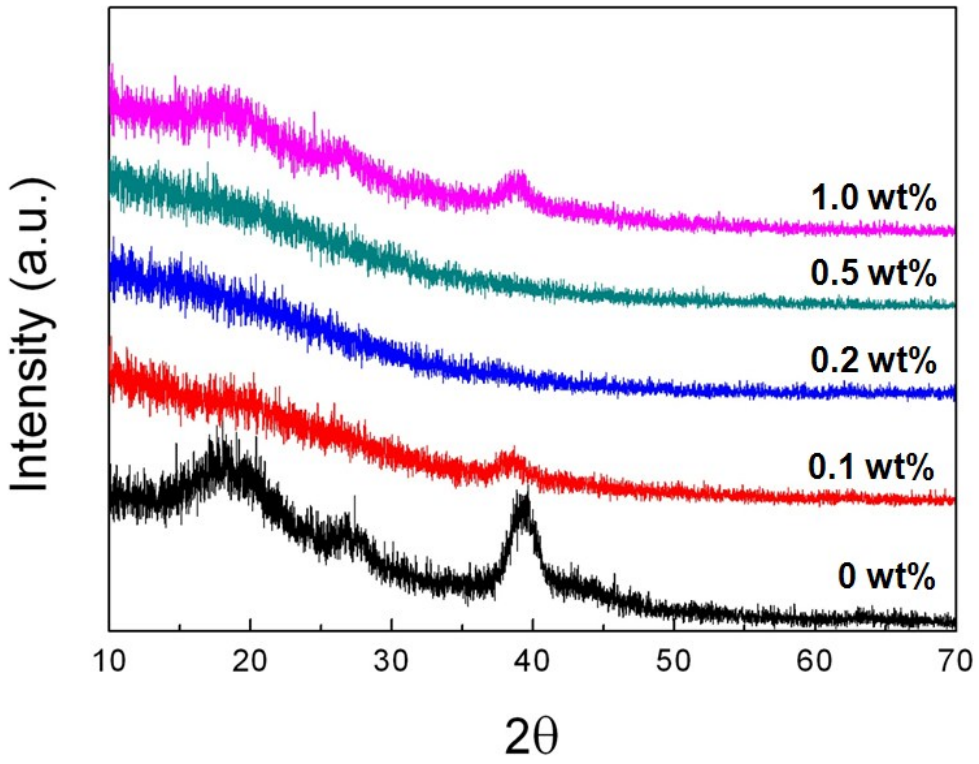

Fig. S13 XRD patterns of CFBNs with 0, 0.1, 0.2, 0.5, and 1.0 wt% of FBN.

As shown in Fig. S13, pristine PVH without FBN has four crystalline peaks ascribed from the alignment of PVH chains. The intensity of the peaks continuously decreases as the FBN content increases up to 0.5 wt%, because the FBN disrupts the alignment of PVH chains, thereby converting the crystalline structure of PVH to amorphous phase. However, crystalline peaks appear again when the FBN content further increases to 1.0 wt%, because aggregated FBNs (Fig. S12e) cannot effectively decrease the crystalline phase of PVH.

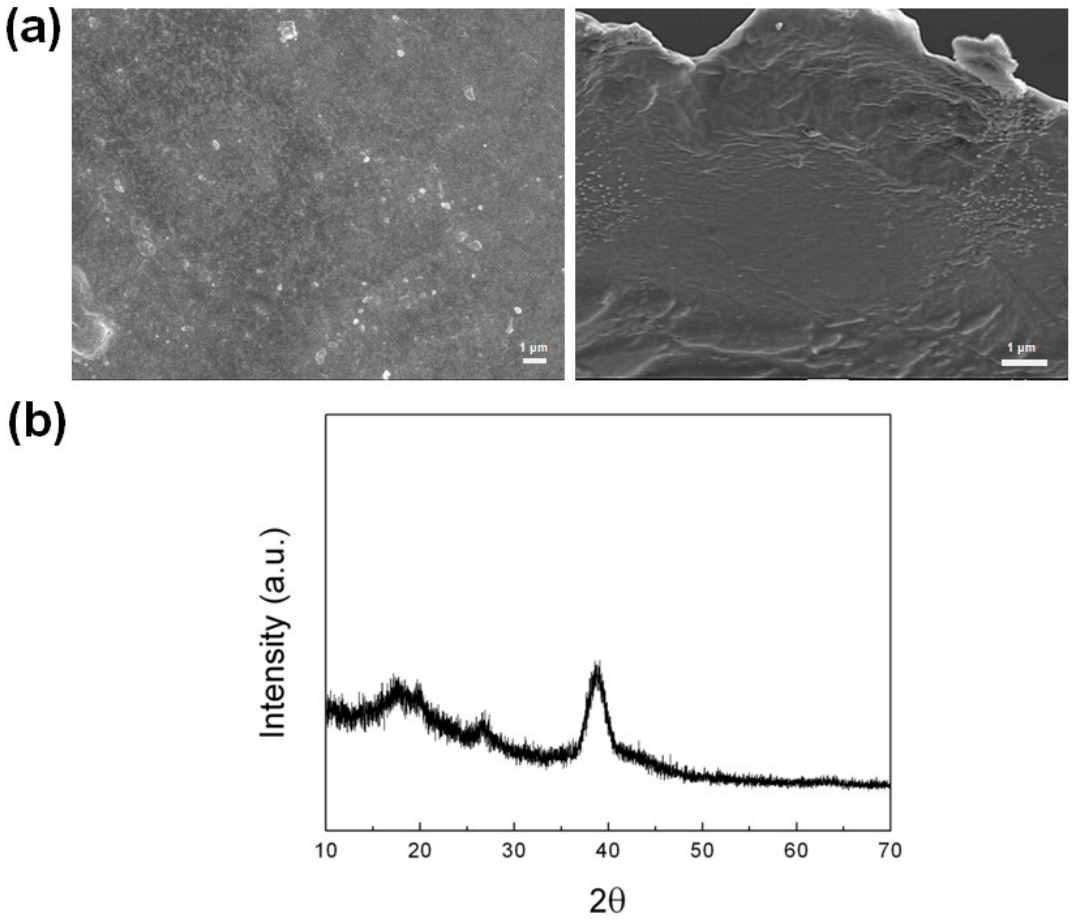

Fig. S14 (a) Surface (left) and cross-sectional (right) SEM images and (b) XRD pattern of CBN with 0.5 wt% BN.

Electrochemical Characterization of Gel Polymer Electrolytes

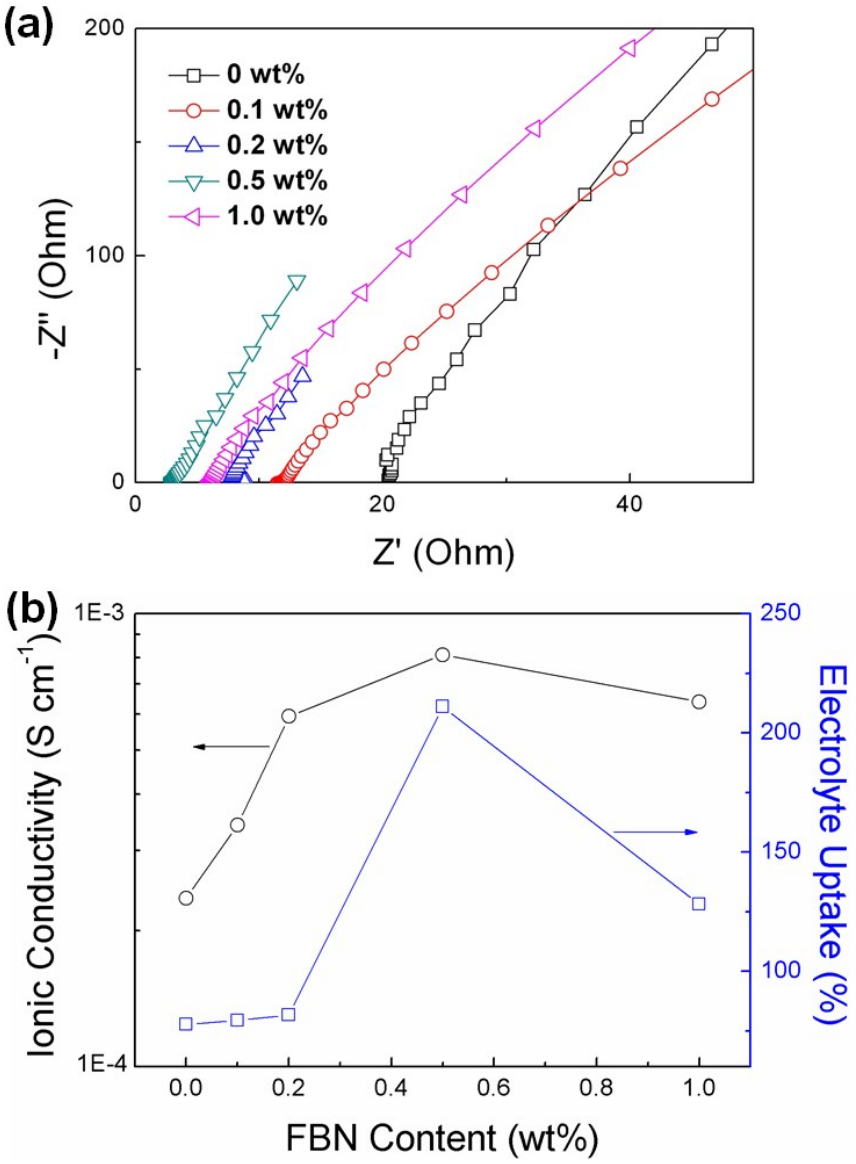

Fig. S15 (a) Electrochemical impedance spectra and (b) ionic conductivities of G-CFBNs with 0, 0.1, 0.2, 0.5, and 1.0 wt% FBN.

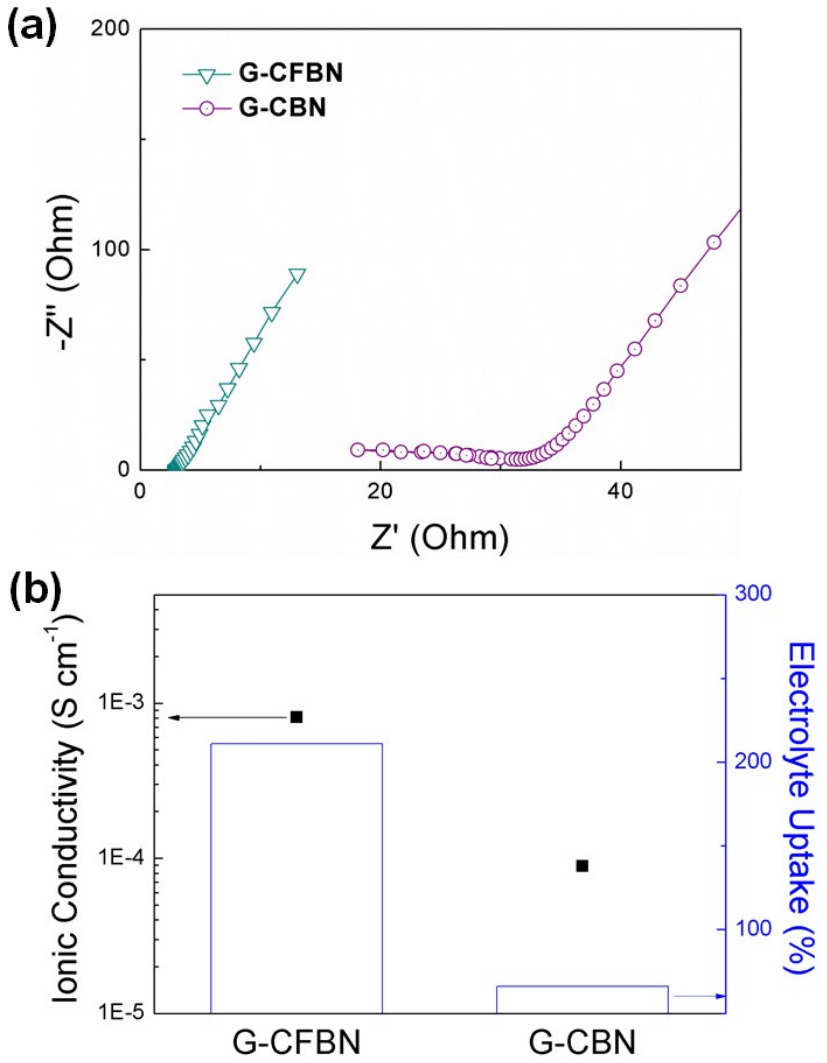

Fig. S16 (a) Electrochemical impedance spectra and (b) ionic conductivity and electrolyte uptake values of G-CFBN and G-CBN.

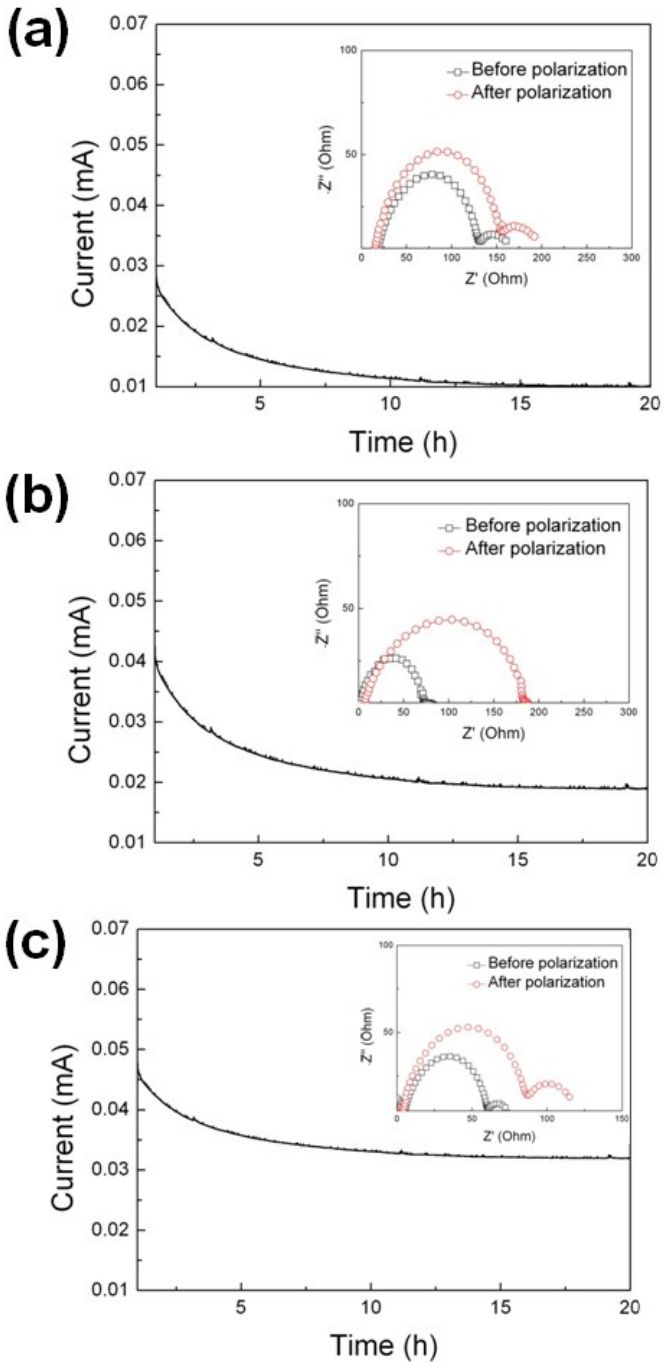

Fig. S17 Chronoamperometric curves of Li/electroltye/Li cells, where the electrolyte is (a) LE-Celgard, (b) G-PVH, and (c) G-CFBN.

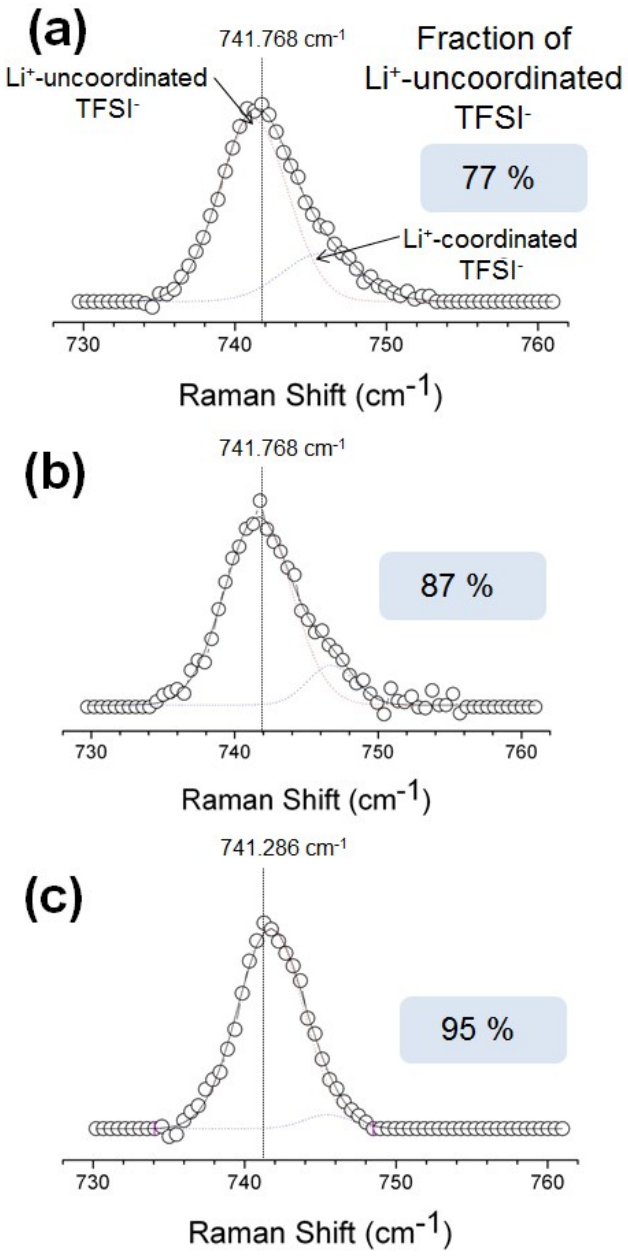

Fig. S18 Raman spectra of (a) LE-Celgard, (b) G-PVH, and (c) G-CFBN.

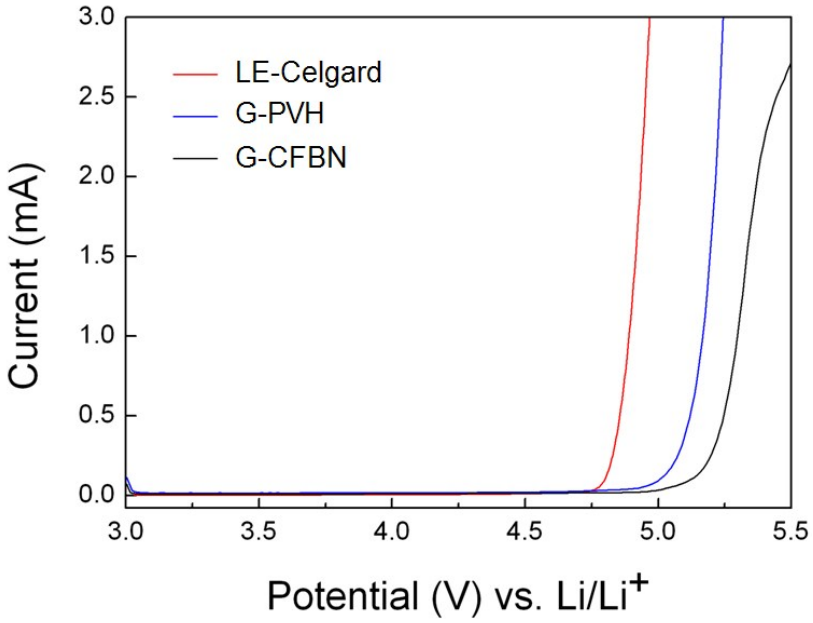

Fig. S19 Linear sweep voltammograms of LE-Celgard, G-PVH, and G-CFBN at 25 °C (scan rate: 1.0 mV s^{-1}).

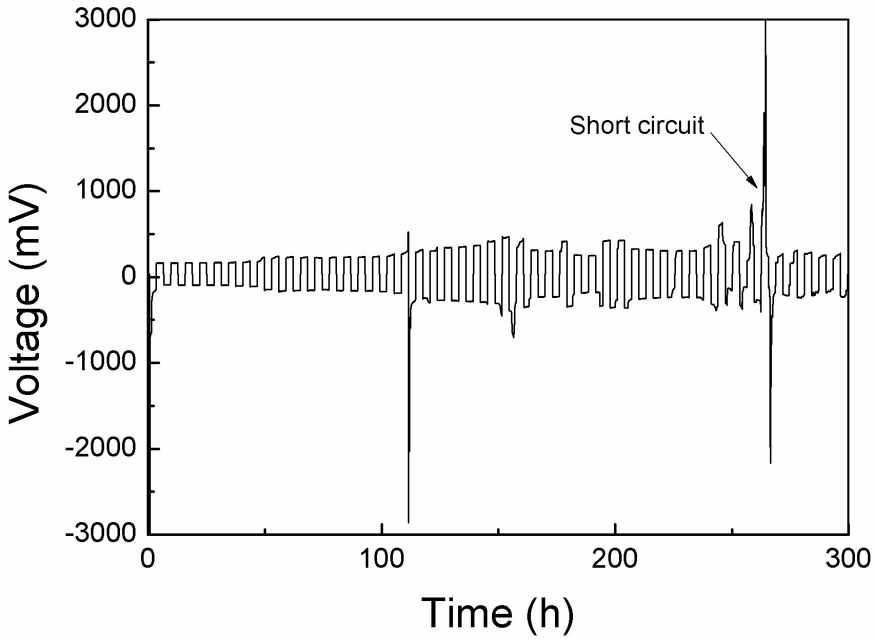

Fig. S20 Galvanostatic cycling profiles of symmetric Li/Li cells with G-PVH (thickness = 24 um) at a current density of 1.0 mA cm^{-2} at 25 °C.

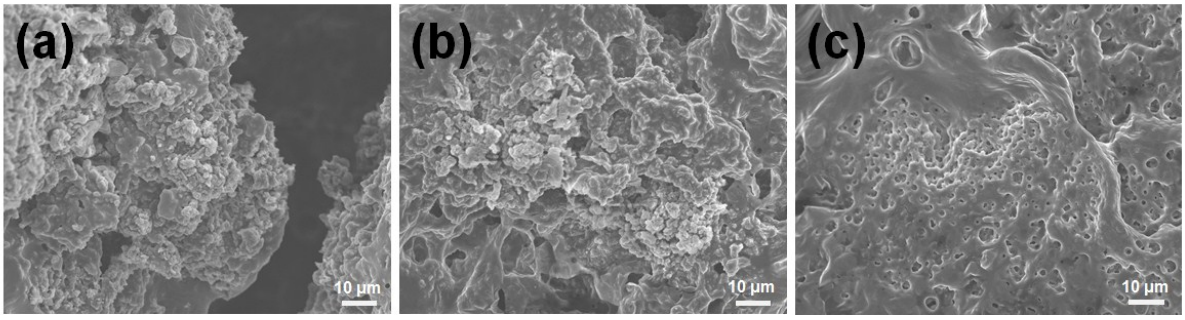

Fig. S21 SEM images of Li metal surface of Li/electrolyte/Li cells after short circuit in galvanostatic cycling test at a current density of 1.0 mA cm^{-2} at 25 ^{o}C, where the electrolyte is (a) G-PVH, (b) LE-Celgard, and (c) G-CFBN.

Table S1 Summary of recent literature reports on galvanostatic cycling test.

Type	Materials	Filler content (wt%)	Current density (mA cm^{-2})	Charge/ discharge time (h)	Temp. (^oC)	Short circuit time (h)	Ref.
GPE	PVdF-HFP/FBN	0.5	1.0	3	25	1940	Present study
GPE /Separator	PVdF-HFP /A-LLTO/m-SiO_2	80	0.48	2	25	1922	S1
	PVdF-HFP /Epoxy resin	-[a]	1.0	3	25	> 600	S2
	PVdF-HFP/ Nanoporous Al_2O_3/PVdF-HFP	-[a]	0.2	3	25	> 1000	S3
	PVdF/Hollow SiO_2/ Crosslinked TPGDA	80	1.0	3	25	> 200	S4
	Silica/ PEO oligomer	6	1.0	3	25	> 100	S5
	Nanoporous Al_2O_3 membrane	-[a]	1.0	1	25	> 1560	S6
	Poly(*p*-phenylene benzobisoxazole) nanofiber	-[a]	0.38	3	25	> 700	S7
SPE	Crosslinked PEG-POSS	-[a]	0.3 0.5 1.0	3	90	> 2600 1212 441	S8
	PEO/LLZO	-[a]	0.5	0.5	25	> 1000	S9

Table S1 (Continued)

Type	Materials	Filler content (wt%)	Current density (mA cm^{-2})	Charge/ discharge time (h)	Temp. (^{o}C)	Short circuit time (h)	Ref.
SPE	Crosslinked PE-PEO/PEG	-[a]	0.26 0.4 0.7 1.0	3	90	275 96 50 27	S10
	PS-*b*-PEO	-[a]	0.02	4	85	180	S11
Li Coating/ Additive	Li/Al_2O_3	-[a]	1.0	0.25	25	> 600	S12
	Li/PI-ZnO	-[a]	1.0	1	25	> 200	S13
	Li/PVdF/Nafion	-[a]	1.1	1	25	> 200	S14
	Li/GO	-[a]	0.5	3	25	7.5	S15
	Li/Kimwipe paper	-[a]	2.0	3	25	> 1000	S16
	Li/Li_3PO_4	-[a]	1.0	1	25	> 300	S17
	Li/rGO	-[a]	1.0	1	25	> 222	S18
	Li/RTIL	-[a]	1.0	0.25	25	> 190	S19
	Li/LiF	-[a]	1.0	4	25	> 1750	S20

[a] No fillers are included. [Abbreviation] A-LLTO: Perovskite-structured aluminum-doped lithium lanthanum titanate; m-SiO2: modified SiO2, PEO: poly(ethylene oxide); TPGDA: tripropylene glycol diacrylate; POSS: polyhedral oligomeric silsesquioxane; LLZO: garnet-type $Li_{6.4}La_3Zr_2Al_{0.2}O_{12}$; PE: polyethylene; PS: polystyrene; RTIL: room-temperature ionic liquid

Mechanical and Thermal Properties of Composite Membranes and Gel Polymer Electrolytes

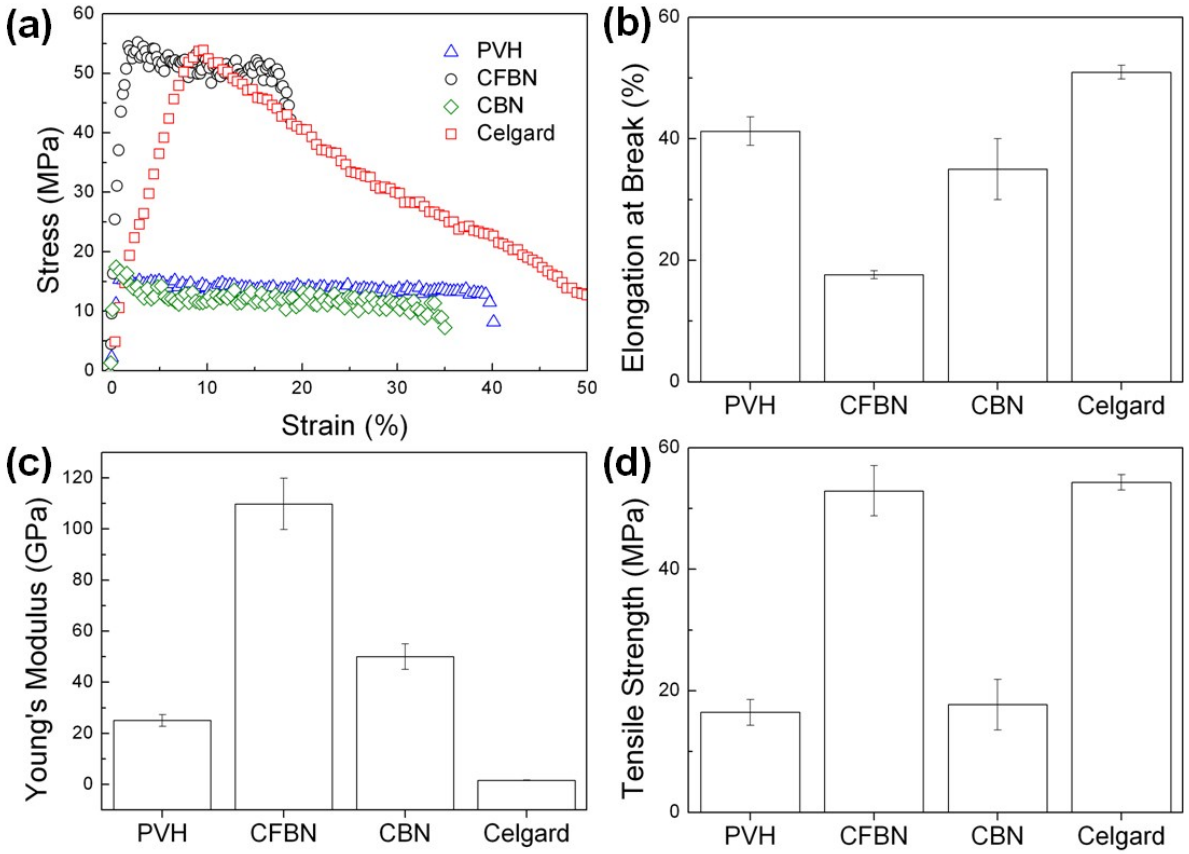

Fig. S22 UTM results of PVH, CFBN, CBN, and Celgard. (a) Stress-strain curves, (b) elongation at break, (c) Young's modulus, and (d) tensile strength.

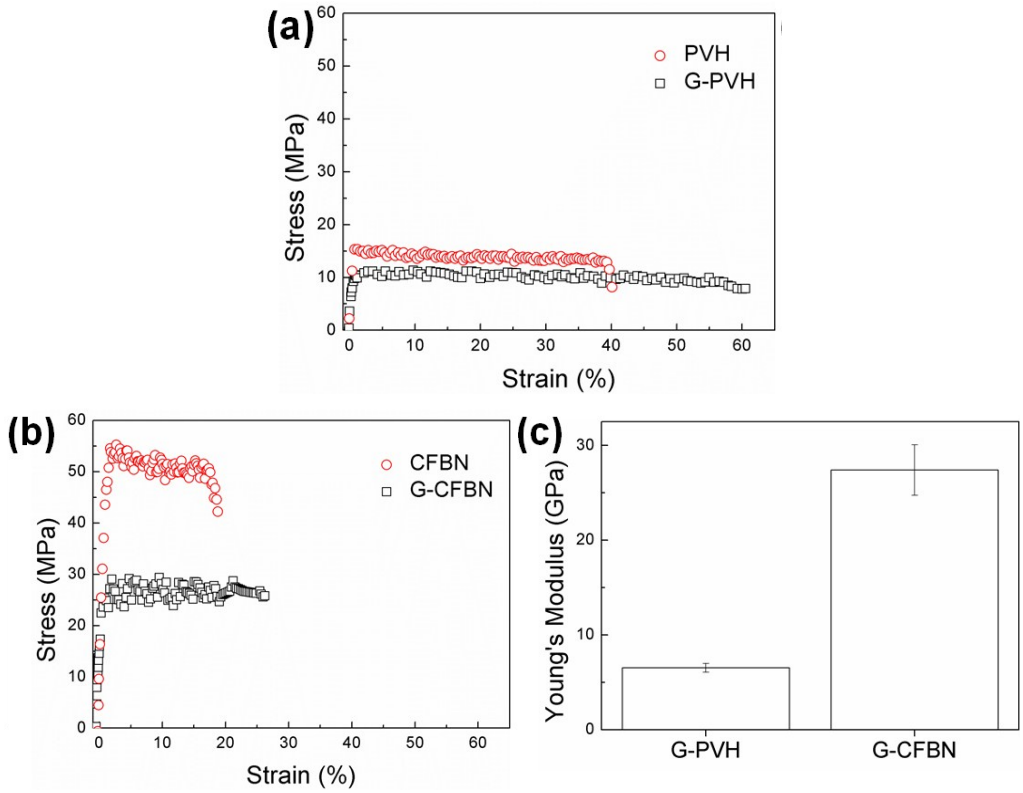

Fig. S23 Stress-strain curves of (a) PVH/G-PVH and (b) CFBN/G-CFBN and (c) Young's modulus of G-PVH and G-CFBN, where electrolyte uptake of G-PVH and G-CFBN is controlled as 60%.

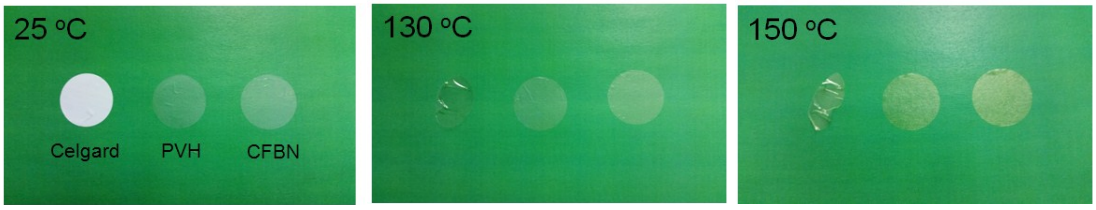

Fig. S24 Thermal stability of Celgard, PVH, and CFBN at 25 °C, 130 °C, and 150 °C.

When Celgard, PVH, and CFBN are placed in an oven thermostatted at certain temperatures (25, 130, and 150 °C) as shown in Fig. S24, Celgard rapidly shrinks over 130 °C due to melting transition of polyolefin (PP/PE/PP), while both PVH and CFBN maintain their pristine state without any thermal shrinkage or melting behaviour due to the intrinsic thermal stability of both PVH matrix and FBN.

Cycling Performance of Li/$LiFePO_4$ Cells with G-CFBN and LE-Celgard

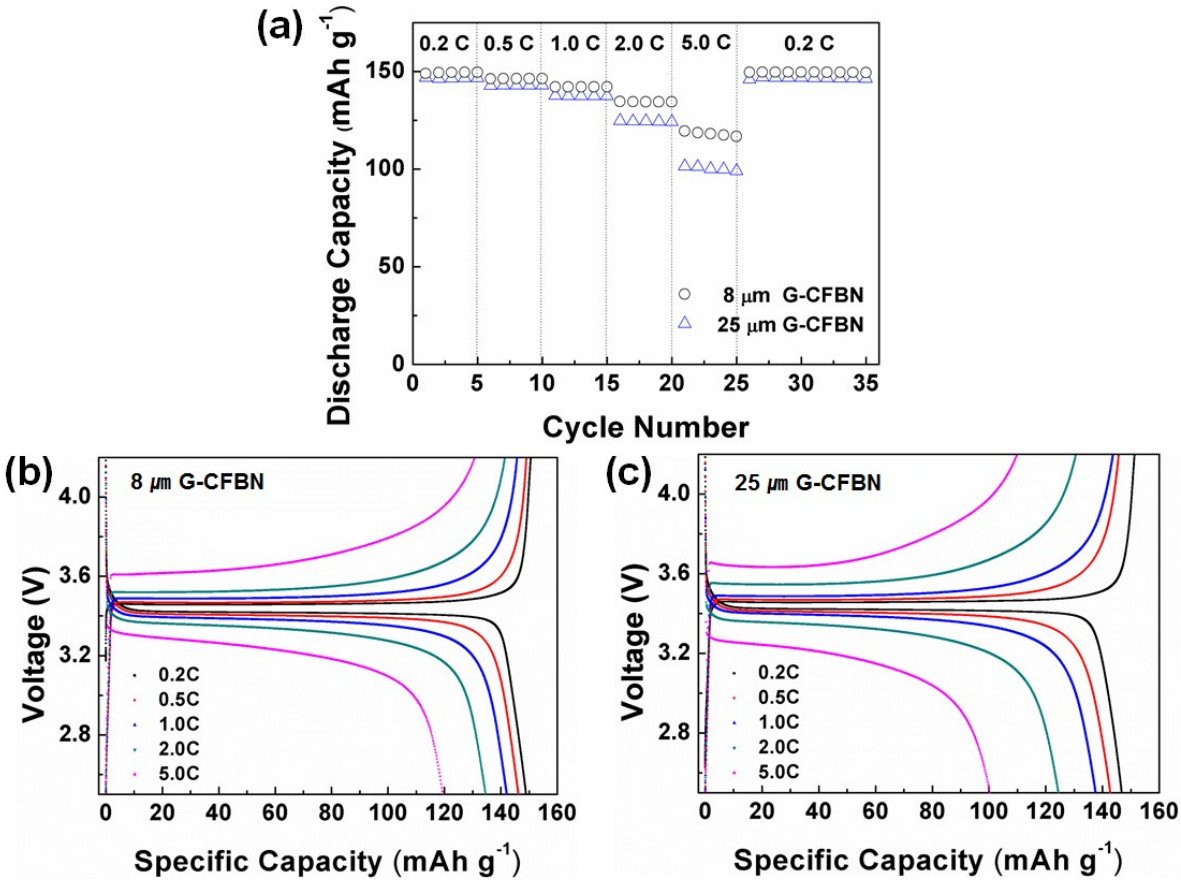

Fig. S25 (a) Rate capability and (b and c) voltage-capacity curves of Li/electrolyte/$LiFePO_4$ cell cycled at 25 °C with various C-rates, where the electrolyte is 8 μm and 25 μm thick G-CFBN.

When the thickness of G-CFBN is increased from 8 um to 25 um by controlling the concentration of casting mixture from 10 wt% to 20 wt%, respectively, discharge capacity values are slightly decreased under various C-rates, because the cycling performance is influenced by total ionic conductance (unit: S = Ω^{-1}) of the electrolyte rather than ionic conductivity (unit: S cm^{-1}) that is normalized by electrolyte thickness. When the thickness of the electrolyte gets thinner, the resistance for ionic conduction decreases, thereby leading to enhanced total ionic conductance for better cycling performance.

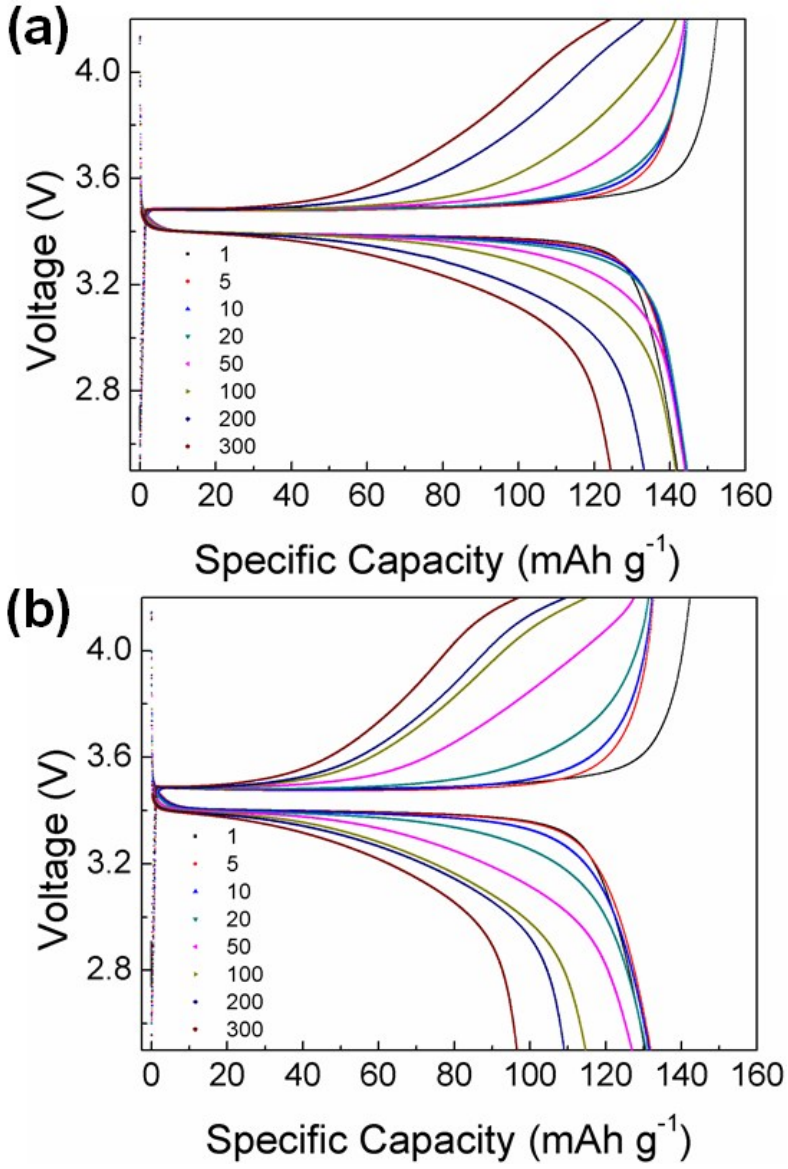

Fig. S26 Voltage-capacity curves of Li/electrolyte/$LiFePO_4$ cells cycled at 25 °C with 1.0 C, where the electrolyte is (a) G-CFBN and (b) LE-Celgard.

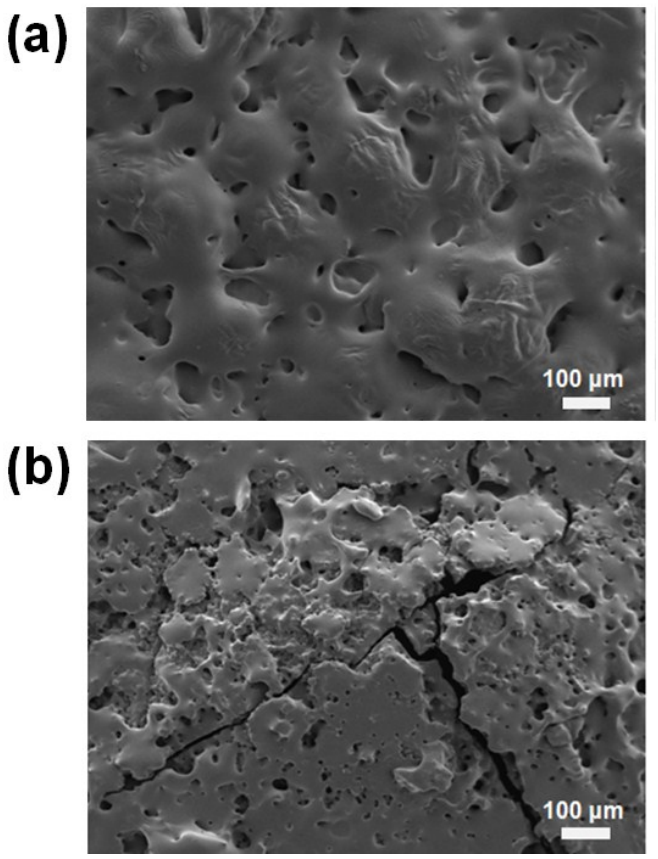

Fig. S27 SEM images of Li metal surface of Li/electrolyte/$LiFePO_4$ cells after 300 cycles at 25 °C with 1.0 C, where the electrolyte is (a) G-CFBN and (b) LE-Celgard.

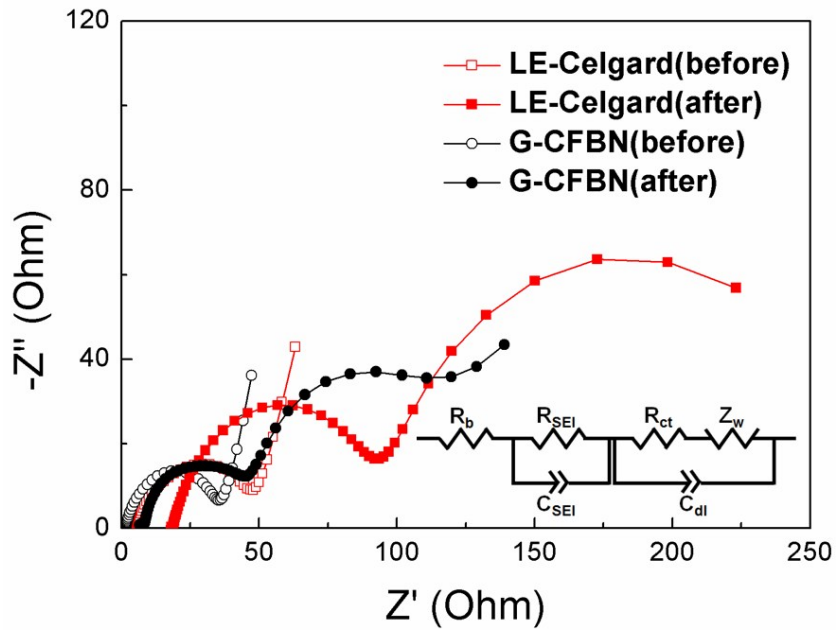

Fig. S28 Electrochemical impedance spectra of Li/electrolyte/$LiFePO_4$ cells before and after 300 cycles at 25 °C with 1.0 C, where the electrolyte is G-CFBN and LE-Celgard.

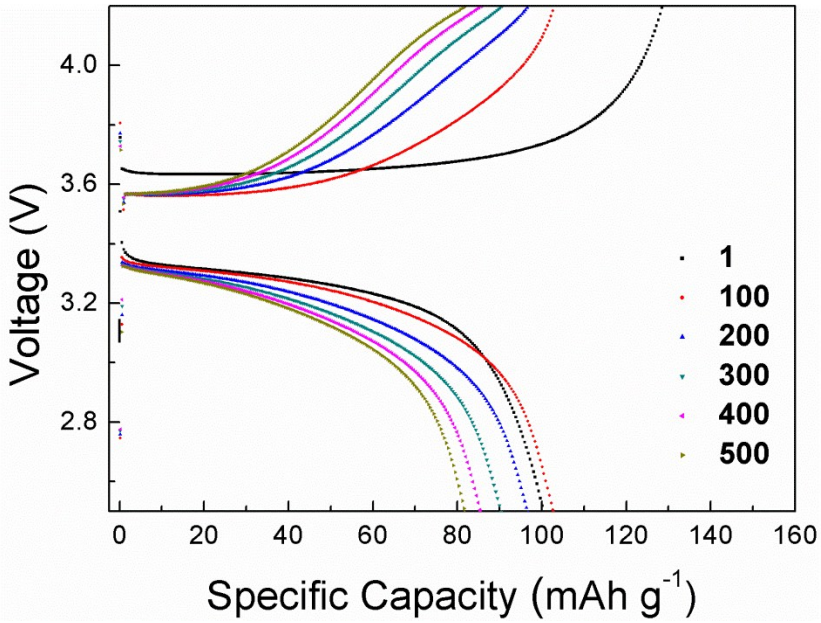

Fig. S29 Voltage-capacity curves of Li/G-CFBN/$LiFePO_4$ cell cycled at 25 °C with 10 C.

Table S2 Summary on cycling performance of LMBs containing GPE from recent literature reports.

Materials	**C-rate**	**Cycle number**	**Cathode (theoretical capacity)**	**Capacity retention (%)**	**Initial capacity /final capacity (mAh g^{-1})**	**Ref.**
PVdF-HFP/FBN	10 C	500	$LiFePO_4$ (170 mAh g^{-1})	82	100/82	Present study
Nonwoven PTFE/poly(methylethyl α-cyanoacrylate)	10 C	5	$LiNi_{0.5}Mn_{1.5}O_4$ (147 mAh g^{-1})	93	70/65	S21
PVdF-HFP /PU/PMMA/SiO_2	10 C	13	$LiFePO_4$ (170 mAh g^{-1})	91	137/125	S22
PVdF-HFP /Epoxy resin	20 C	6	$LiFePO_4$ (170 mAh g^{-1})	91	80/73	S2

PTFE: polytetrafluoroethylene; PU: polyurethane; PMMA: Poly(methyl methacrylate)

There have been a few reports on the LMBs operated under high C-rates over 10 C. Such reports are summarized in Table S2, but it is very difficult to evaluate their cycle performance precisely, because the cells in the literature were not operated over 20 cycles. In our case, capacity is retained as 96 % and 82 % even after 200 and 500 cycles, respectively. To the best of our knowledge, this is the longest operation of LMB with great capacity retention at 10 C rate ever reported.

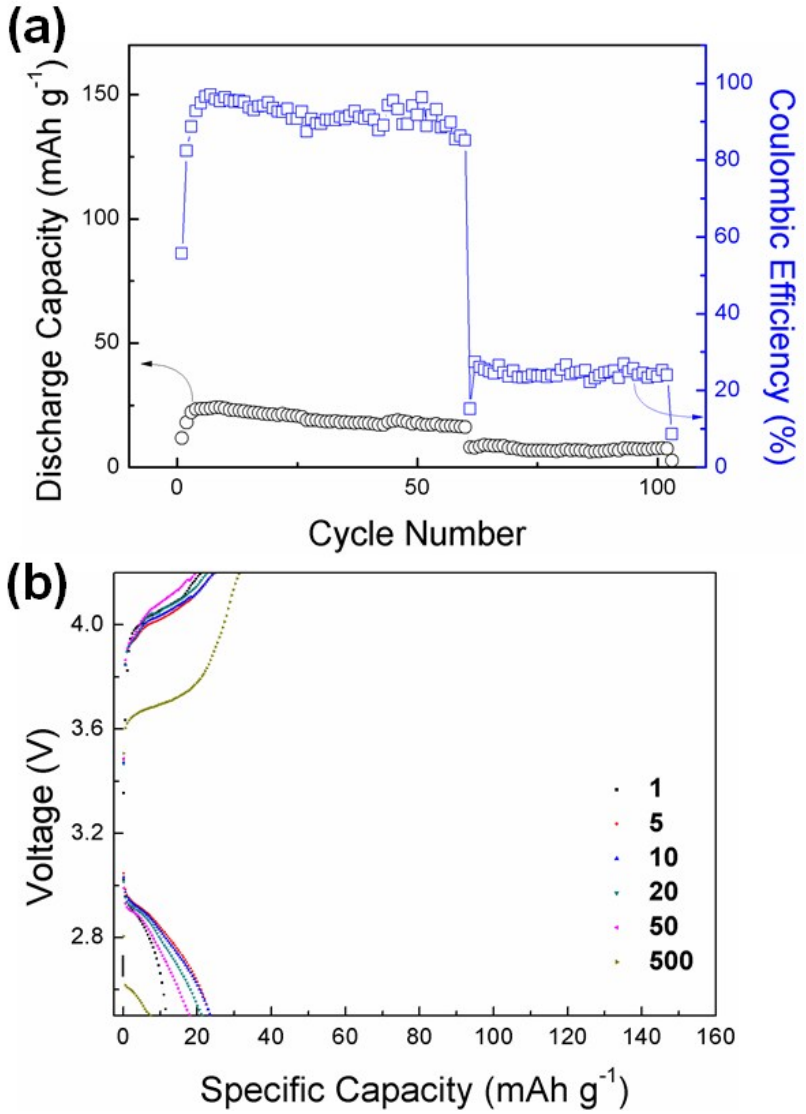

Fig. S30 (a) Long-term cycling performance and (b) voltage-capacity curves of Li/LE-Celgard/$LiFePO_4$ cell cycled at 25 °C with 10 C.

References for Electronic Supplementary Information

(S1) H. T. T. Le, D. T. Ngo, R. S. Kalubarme, G. Cao, C.-N. Park and C.-J. Park, *ACS Appl. Mater. Interfaces* **2016**, *8*, 20710-20719.

(S2) Q. Lu, Y.-B. He, Q. Yu, B. Li, Y. V. Kaneti, Y. Yao, F. Kang and Q.-H. Yang, *Adv. Mater.* **2017**, 1604460.

(S3) Z. Y. Tu, Y. Kambe, Y. Y. Lu and L. A. Archer, *Adv. Energy Mater.* **2014**, *4*, 1300654.

(S4) D. Zhou, R. Liu, Y.-B. He, F. Li, M. Liu, B. Li, Q.-H. Yang, Q. Cai and F. Kang, *Adv. Energy Mater.* **2016**, *6*, 1502214.

(S5) S. Choudhury, R. Mangal, A. Agrawal and L. A. Archer, *Nat. Commun.* **2015**, *6*, 10101.

(S6) Z. Tu, M. J. Zachman, S. Choudhury, S. Wei, L. Ma, Y. Yang, L. F. Kourkoutis and L. A. Archer, *Adv. Energy Mater.* **2017**, 1602367.

(S7) X. M. Hao, J. Zhu, X. Jiang, H. T. Wu, J. S. Qiao, W. Sun, Z. H. Wang and K. N. Sun, *Nano Lett.* **2016**, *16*, 2981-2987.

(S8) Q. W. Pan, D. M. Smith, H. Qi, S. J. Wang and C. Y. Li, *Adv. Mater.* **2015**, *27*, 5995-6001.

(S9) K. Fu, Y. H. Gong, J. Q. Dai, A. Gong, X. G. Han, Y. G. Yao, C. W. Wang, Y. B. Wang, Y. N. Chen, C. Y. Yan, Y. J. Li, E. D. Wachsman and L. B. Hu, *Proc. Natl. Acad. Sci. USA* **2016**, *113*, 7094-7099.

(S10) Q. Zheng, L. Ma, R. Khurana, L. A. Archer and G. W. Coates, *Chem. Sci.* **2016**, *7*, 6832-6838.

(S11) N. S. Schauser, K. J. Harry, D. Y. Parkinson, H. Watanabe and N. P. Balsara, *J. Electrochem. Soc.* **2015**, *162*, A398-A405.

(S12) E. Kazyak, K. N. Wood and N. P. Dasgupta, *Chem. Mater.* **2015**, *27*, 6457-6462.

(S13) Y. Y. Liu, D. C. Lin, Z. Liang, J. Zhao, K. Yan and Y. Cui, *Nat. Commun.* **2016**, *7*, 10992.

(S14) J. Luo, R.-C. Lee, J.-T. Jin, Y.-T. Weng, C.-C. Fang and N.-L. Wu, *Chem. Commun.* **2017**, *53*, 963-966.

(S15) Y. J. Zhang, X. H. Xia, X. L. Wang, C. D. Gu and J. P. Tu, *RSC Adv.* **2016**, *6*, 66161-66168.

(S16) C.-H. Chang, S.-H. Chung and A. Manthiram, *Adv. Sustainable Syst.* **2017**, *1*, 1600034.

(S17) L. Wang, Q. Wang, W. Jia, S. Chen, P. Gao and J. Li, *J. Power Sources* **2017**, *342*, 175-182.

(S18) D. Lin, Y. Liu, Z. Liang, H.-W. Lee, J. Sun, H. Wang, K. Yan, J. Xie and Y. Cui, *Nat. Nano* **2016**, *11*, 626-632.

(S19) A. Basile, A. I. Bhatt and A. P. O'Mullane, *Nat. Commun.* **2016**, *7*, 11794.

(S20) S. Choudhury and L. A. Archer, *Adv. Electron. Mater.* **2016**, *2*, 1500246.

(S21) J. Chai, J. Zhang, P. Hu, J. Ma, H. Du, L. Yue, J. Zhao, H. Wen, Z. Liu, G. Cui and L. Chen, *J. Mater. Chem. A* **2016**, *4*, 5191-5197.

(S22) Z. He, Q. Cao, B. Jing, X. Wang and Y. Deng, *RSC Adv.* **2017**, *7*, 3240-3248.